Water Research 286 (2025) 124063

Contents lists available at ScienceDirect

Water Research

journal homepage: www.elsevier.com/locate/watres

Combining field datasets and mathematical modeling to quantify PFAS leaching and mass discharge at an AFFF-impacted site

Ryan Russell [a], Bo Guo [a,*], Jicai Zeng [a], Mark L. Brusseau [a,b], Charles E. Schaefer [c], Stefanie Shea [d], Christopher P. Higgins [d], Ty P.A. Ferre [a]

[a] Department of Hydrology and Atmospheric Sciences, University of Arizona, United States of America
[b] Department of Environmental Science, University of Arizona, United States of America
[c] CDM Smith, United States of America
[d] Department Civil and Environmental Engineering, Colorado School of Mines, United States of America

ARTICLE INFO

Keywords:
Per- and polyfluoroalkyl substances (PFAS)
Rate-limited desorption
Vadose zone
Groundwater
Mass discharge
Mathematical modeling

ABSTRACT

Vadose zones serve as significant reservoirs of per- and polyfluoroalkyl substances (PFAS) at contaminated sites, posing risks to the groundwater underneath. Partitioning of PFAS to the solid–water and air–water interfaces in soils complicates PFAS leaching in the vadose zone. We apply mathematical models representing PFAS-specific retention and transport processes to simulate vadose-zone leaching and mass discharge at a PFAS-contaminated field site. The mathematical models are constrained by detailed datasets collected at the site under both ambient rainfall and artificial flushing conditions. Predicted porewater concentrations generally agree with those sampled by suction lysimeters over a period of 2 months. Model-based analysis suggests: (1) minimal downward migration of PFOS and PFOA occurred over the 2-month period, (2) variations in observed porewater concentrations were caused by mass redistribution among the different phases in response to dynamic changes in soil moisture content and air–water interfacial area, (3) accounting for rate-limited solid-phase desorption reduces discrepancies between simulated and sampled porewater concentrations for PFOS and PFOA, particularly for the shallowest depth interval, and (4) porewater concentration and moisture data may be used to estimate air–water interfacial area. Additional 40-year long-term simulations indicate that the simulated leaching is consistent with field observations for PFOS, but it generally overestimates the leaching for PFOA, PFHxS, and PFBS, which appears to be caused by the simulations not accurately representing desorption kinetics, underestimating solid-phase adsorption, and/or not accounting for precursor transformation. Our results suggest that accurate quantification of source strength and mass discharge at a PFAS-contaminated site requires characterizing hydraulic and transport parameters especially kinetic solid-phase desorption behaviors, PFAS soil concentration profiles, precursor transformation, and site-specific infiltration rates.

1. Introduction

Per- and polyfluoroalkyl substances (PFAS) are a group of contaminants that have been widely used in a variety of manufactured products since the 1950s (ITRC, 2023). The widespread use of PFAS has led to their ubiquitous presence in the environment. A growing body of site investigations have determined that the vadose zone retains a large portion of the PFAS released into the subsurface, suggesting that the vadose zone may represent a significant source for long-term leaching of PFAS contamination to groundwater. The United States Environmental Protection Agency (US EPA) recently finalized National Primary Drinking Water Regulations (NPDWR) for six PFAS (USEPA, 2024), which highlights the importance of understanding and quantifying the mechanisms controlling long-term leaching and mass discharge of PFAS from the vadose zone to groundwater.

Quantifying PFAS leaching in the vadose zone is challenging due to the relatively unique transport properties of PFAS that differ from traditional non-surfactant contaminants. As surfactants, many PFAS adsorb at air–water interfaces in variably-saturated soils, which may greatly increase their retention in the vadose zone. Adsorption at solid–water interfaces due to hydrophobic and electrostatic interactions also contributes to PFAS retention in the vadose zone. Recent desorption experiments on field soils historically exposed to aqueous film-forming foams (AFFF) suggest that a fraction of the PFAS adsorbed at the solid surfaces may not be “readily desorbable” under shorter-term time scales (e.g., weeks to months), indicating the presence of rate-limited

* Corresponding author.
E-mail address: boguo@arizona.edu (B. Guo).

https://doi.org/10.1016/j.watres.2025.124063
Received 19 February 2025; Received in revised form 25 May 2025; Accepted 20 June 2025
Available online 18 July 2025

desorption processes (Schaefer et al., 2021, 2022). The transport mechanisms described above may vary for different PFAS due to differences in molecular composition or size such as chain length, charge, or functional group (e.g., Guelfo and Higgins, 2013; Brusseau et al., 2019; Brusseau, 2023b).

Mathematical models accounting for PFAS-specific retention and transport processes in the vadose zone with varying complexities have been developed (e.g., Guo et al., 2020; Silva et al., 2020; Guo et al., 2022; Zeng and Guo, 2021; Wallis et al., 2022; Zeng and Guo, 2023; Smith et al., 2024). While some of these models have been validated by miscible-displacement experiments using packed soil columns (e.g., Zeng et al., 2021; Brusseau et al., 2021; Guo et al., 2022; Liao et al., 2022; Stults et al., 2022; Garza-Rubalcava et al., 2024; Vahedian et al., 2024) and parameterized to simulate the leaching of contaminated packed soils (Stults et al., 2024), applications to field PFAS-contaminated sites are limited (Wallis et al., 2022; Ruyle et al., 2023; Bigler et al., 2024; Arshadi et al., 2024), and no direct comparisons with or validations by field observations such as porewater concentrations have been reported.

At PFAS-contaminated sites, suction lysimeters have been increasingly used to sample and obtain porewater PFAS concentration in the vadose zone (e.g., Quinnan et al., 2021; Anderson, 2021; Schaefer et al., 2022, 2023; Anderson et al., 2022). These datasets and simple mass-balance-based analyses provide critical insights (Brusseau and Guo, 2022; Schaefer et al., 2022), but they have not been used to constrain and improve the application of mathematical modeling at PFAS-contaminated field sites. The availability of soil porewater PFAS concentrations in conjunction with detailed site characterization and hydrological sampling (Schaefer et al., 2019, 2021, 2022; Schaefer et al., 2022, 2023) provides opportunities to test and demonstrate the applicability of mathematical models for quantifying PFAS leaching and mass discharge at PFAS-contaminated sites.

The present work represents one of the first studies that combines detailed field data collected at an AFFF-impacted site (Schaefer et al., 2022, 2023) with mathematical models (Guo et al., 2020) that account for a variety of PFAS-specific retention and transport processes to quantify PFAS leaching and mass discharge from the vadose zone to groundwater. The objectives of the study are: 1) test and evaluate the applicability of mathematical models for simulating PFAS leaching and transport in the vadose zone, 2) analyze and identify the primary factors controlling PFAS leaching in the vadose zone at contaminated sites, and 3) provide guidance for future field investigations that aim to employ mathematical models for estimating PFAS leaching and mass discharge from the vadose zone to groundwater.

2. Method

We study an AFFF-impacted site located in the northeastern United States where detailed datasets have been collected in prior efforts (Schaefer et al., 2022, 2023). In this section, we first present basic information about the AFFF-impacted site and the various datasets collected (Section 2.1). We then introduce the mathematical modeling approach (Section 2.2), including the design of the numerical simulations, the determination of model parameters, and the approaches to analyze the simulation results.

2.1. AFFF-impacted site and the datasets collected

The AFFF-impacted site is located at the Joint Base McGuire-Dix-Lakehurst and was contaminated by PFAS due to foam formulation testing (not the application of AFFF for firefighting training). The last known application of AFFF at the site occurred approximately in 1997. The depth to groundwater typically ranges from 1.8 to 2.7 meters (m) below ground surface (bgs) (Schaefer et al., 2022).

A highly characterized and instrumented 4.3 m × 4.3 m test cell was established at the AFFF-impacted site. A schematic of the test cell showing the locations of soil borings, soil porewater sampling lysimeters, and soil moisture probes (SMPs) is presented in Fig. 1. From 2019 to 2024, a wide range of datasets have been collected at the test cell. In 2019, soil cores were sampled and sent for laboratory analysis to delineate the extent of PFAS contamination and assist research efforts in evaluating PFAS desorption from vadose zone soils (Schaefer et al., 2021, 2022). Measured PFAS concentrations of the collected soil cores are presented in Fig. 2, which were not reported in the original studies of Schaefer et al. (2021, 2022). The tabulated concentration data are presented in Table S1 in the Supplementary Data (Appendix A). Laboratory analysis of the soil physical properties of the collected soil cores are provided in Table S2 in the Supplementary Data (Appendix A). Measured grain size percentages indicate that the soil within the test cell is approximately 92% sand, 3% gravel, and 5% silt. Approximately 1.5 years after soil core sampling, a network of porewater sampling lysimeters and SMPs were installed at various depths. The measurement and sampling depths of each lysimeter and SMP are presented in Table 1. An on-site rain gauge was installed to monitor precipitation. However, due to a later date of installation and time gaps in operation, the rain gauge data does not cover the entire period of investigation. Whenever on-site rain gauge data are unavailable, we use a nearby weather station, approximately 40 km from the site, to estimate daily precipitation. The rainfall datasets from the off-site and on-site stations agree well for the periods when they are both available (See Figure S2 in the Supplementary Data (Appendix A)). Using soils collected from the test cell site, Schaefer et al. (2021, 2022) determined site-specific solid-phase desorption coefficient values (K_d) and fractions of the PFAS adsorbed at solid surfaces that were not readily desorbable over the time scale of their desorption experiments (which indicates rate-limited desorption).

Field data were collected under both ambient rainfall (Dataset 1) and simulated flushing (Dataset 2) conditions. The observational period under ambient rainfall conditions lasted approximately 53 days, during which soil moisture was continuously measured and three separate soil porewater sampling events were conducted. The soil moisture data and time intervals corresponding to each sampling event for Dataset 1 are presented in Fig. 3. During each sampling event, a vacuum was applied during or shortly after a rainfall event over a time period ranging from approximately 18 hours to 5 days to ensure adequate sample volume (Schaefer et al., 2021; Schaefer et al., 2022). Simulated flushing was applied after the investigation under ambient rainfall conditions. The flushing was accomplished using nine sprinklers installed within the test cell and lasted for two hours each morning at a rate of approximately 77 centimeters per day (cm/d). Soil moisture data were continuously collected over the entire course (approximately 456 days) of the flushing experiments. The soil moisture data collected from three SMP locations installed at varying depths (SMP-1, SMP-2, and SMP-3; see Table 1) are used for mathematical modeling. Additional details on how the soil moisture data are post-processed are presented in Section S1 of the Supplementary Data (Appendix A).

2.2. Mathematical modeling of variably-saturated flow and PFAS transport

We construct three separate 1D model domains (MD-1 to MD-3) as three realizations of the vadose zone at the test cell (Fig. 4), corresponding to the information collected at the three soil moisture probe locations in Fig. 1. For each 1D model domain and the corresponding soil moisture dataset, we employ HYDRUS-1D (Šimůnek et al., 2013) to inversely estimate soil hydraulic parameters using a subset of the soil moisture data. Then, we conduct forward predictions using the calibrated parameters and compare the results to a separate subset of soil moisture data for model evaluation. More details on the determination of model parameters are described in Section 2.2.1. Note that HYDRUS-1D is only used for inverse modeling of variably saturated water flow to estimate hydraulic parameters. All the other simulations

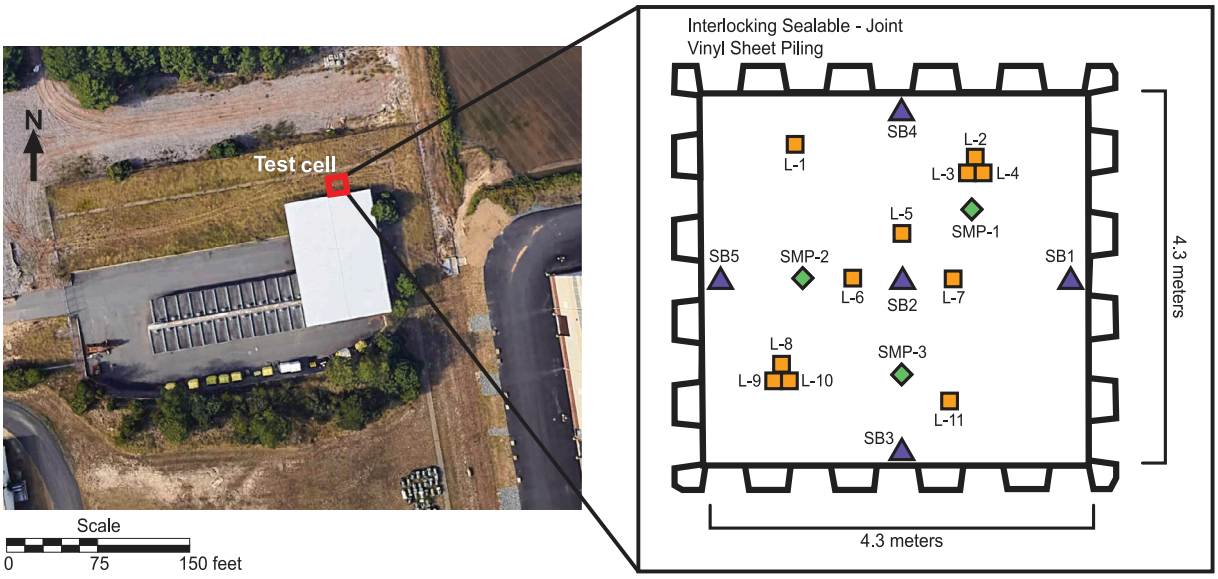

Fig. 1. AFFF-impacted site location and schematic for the instrumentation of the test cell (Schaefer et al., 2022) with locations of soil borings (SB), soil porewater sampling lysimeters (L), and soil moisture probes (SMP). Two clusters of porewater sampling lysimeters are nested (L-2, L-3, and L4; and L-8, L-9, and L-10; see also Table 1).

Table 1
Measurement and sampling depths of the lysimeters and soil moisture probes installed within the test cell. The lysimeters that are part of two nested clusters are marked by "*". Source: Schaefer et al. (2022).

Location	L-1	L-2*	L-3*	L-4*	L-5	L-6	L-7	L-8*	L-9*	L-10*	L-11	SMP-1	SMP-2	SMP-3
Depth (cm bgs)	61	15	61	150	61	150	120	15	61	120	61	100	20, 60	100

in the present study (including PFAS transport) are conducted using the comprehensive model of Guo et al. (2020).

With the soil hydraulic parameters determined from inverse modeling, the PFAS transport and desorption parameters obtained from laboratory studies (Schaefer et al., 2021, 2022), and the literature, we then simulate the leaching and mass discharge of four PFAS present at the site (PFOS, PFOA, PFBS, and PFHxS) using the comprehensive mathematical model developed by Guo et al. (2020). The mathematical model accounts for transient variably saturated flow, surfactant-induced flow, advection and dispersion of PFAS, and nonlinear and kinetic adsorption of PFAS at the air–water and solid–water interfaces. Additional details on the mathematical formulations and numerical methods can be found in Guo et al. (2020).

We conduct two distinct modeling scenarios. The first scenario covers 60 days (i.e., short-term) and evaluates the mathematical model by comparing the predicted porewater concentrations against the suction lysimeter data. The second scenario simulates 40 years of PFAS leaching at the site to analyze and identify the primary factors controlling long-term leaching and mass discharge of PFAS from the vadose zone. Additional descriptions of the modeling framework for simulating PFAS leaching and mass discharge to groundwater are presented in Section 2.2.2.

2.2.1. Determination of soil hydraulic parameters and initial soil moisture

We determine the soil hydraulic parameters for model domains MD-1, MD-2, and MD-3 via inverse modeling using the soil moisture data collected at SMP-1, SMP-2, and SMP-3, respectively. The vadose zone at the test cell site was reported to be relatively homogeneous (Schaefer et al., 2022). Based on this information and the fact that there was only one soil moisture probe at one depth for MD-1 and MD-3, these two 1D domains are assumed to be homogeneous. The SMP-2 location has soil moisture probes at two depths. Thus, we have considered two cases for MD-2. One assumes a homogeneous 1D domain, and the other assumes a two-layer heterogeneous 1D domain. The interface location for the 2 layers is part of the inverse modeling process. The 2-layer 1D domain gives better agreement with the measured soil moisture data than the homogeneous 1D domain. As a result, we have selected the 2-layer model for the MD-2 1D model domain.

Subsets of Dataset 1 (ambient rainfall) and Dataset 2 (enhanced flushing) from the three SMP locations (Fig. 3 and Fig. S1 in the Supplementary Data (Appendix A)) were used for the calibration and validation of each corresponding 1D model, respectively. We obtain the initial soil moisture from measured values at 20 cm bgs, 60 cm bgs, and 100 cm bgs with linear interpolation for the rest of the domain. SMP-2 data at 20 cm and 60 cm were used to initialize soil moisture in all three model domains. SMP-1 data were used to initialize soil moisture in MD-1 and MD-2 at 100 cm while SMP-3 data were used to initialize soil moisture in MD-3 at 100 cm. A time-variable atmospheric boundary condition is applied to the upper boundary using on-site rain gauge data (accounting for the added irrigation when it was applied) or rain gauge data from a nearby weather station when the on-site rain gauge was not operational. The rainfall data from the nearby weather station and the on-site rain gauge agree well for the periods when they are both available (See Figure S2 in the Supplementary Data (Appendix A)), which supports the use of the weather station in the absence of on-site rain gauge data. Historical water table depth data at the site show that the water table ranged from 180 to 270 cm bgs (Schaefer et al., 2022). We define the total length of each 1D model domain as 150 cm and apply a free drainage condition at the bottom boundary.

For the inverse modeling, we obtain the initial guesses of soil hydraulic parameters using the Rosetta 3 model (Zhang and Schaap, 2017) based on the geotechnical analysis of the soils collected at the site (see Table S2 in the Supplementary Data (Appendix A)). We set 2 standard deviations (determined by the Rosetta 3 model) from the mean as the upper and lower bounds for each parameter. We perturb the initial guess of each soil hydraulic parameter and repeat the inverse modeling process until these parameters stabilize.

We then validate the calibrated soil hydraulic parameters by conducting forward simulations and comparing the simulated soil moisture to a subset of Dataset 2 (Fig. S1 in the Supplementary Data (Appendix

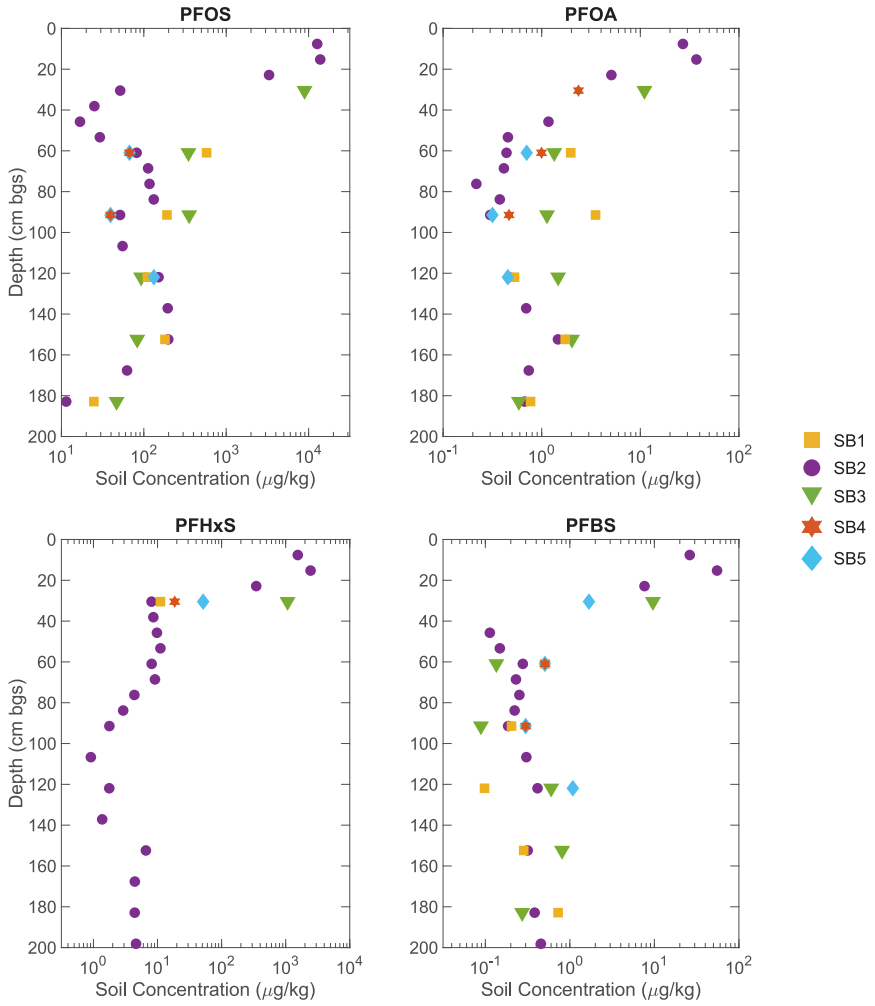

Fig. 2. Profiles of PFAS concentrations (PFOS, PFOA, PFHxS, and PFBS) in soil collected from five soil borings (SB1–SB5) at the 4.3 m × 4.3 m test cell.

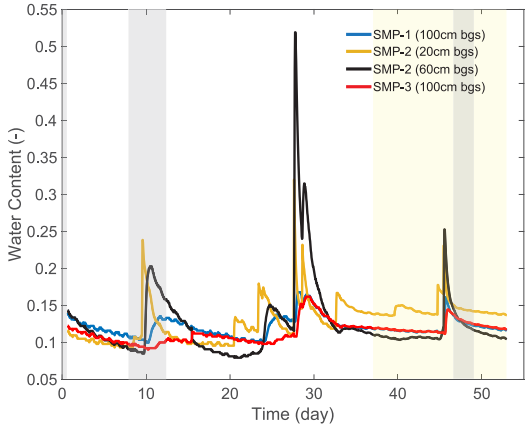

Fig. 3. Soil moisture data collected by four soil moisture probes (SMPs) at three locations within the test cell. The SMPs at locations 1 and 3 were installed at a depth of 100 cm, and location 2 has two soil moisture probes at two depths: 20 cm and 60 cm. Gray bars indicate the time intervals during which soil porewater was sampled by suction lysimeters. The yellow bar indicates the soil moisture data used for determining soil hydraulic parameters via model calibration. The soil moisture datasets were previously reported in Schaefer et al. (2022). (For interpretation of the references to color in this figure legend, the reader is referred to the web version of this article.)

A)). The final, inversely-obtained soil hydraulic parameters for MD-1, MD-2, and MD-3 are presented in Table 3. The resulting soil water characteristics and A_{aw} as a function of water saturation (computed from Eq. (1)) for MD-1 to MD-3 as well as for each set of parameters derived from Rosetta 3 are presented in Fig. S6 in the Supplementary Data (Appendix A).

To assess the sensitivity of the estimated parameters to potential errors in the soil moisture data (e.g., due to probe installation or other sources), we perturb the measured soil moisture data by 50% of the typical expected errors of the PR2/6 soil moisture probes, as defined by Devices (2016). We repeat the calibration process using the perturbed soil moisture data and compare the estimated parameters with the parameters obtained using the original soil moisture data.

A critical parameter impacting PFAS transport in the vadose zone is the air–water interfacial area. Several methods can be employed to estimate the air–water interfacial area. One of the approaches is the thermodynamic-based method that estimates the specific air–water interfacial area A_{aw} using the soil water characteristics (Leverett, 1941; Morrow, 1970) as

$$A_{aw} = \frac{\phi}{\sigma}\int_{S_w}^{1} p_c \mathrm{d}S_w, \tag{1}$$

where S_w is water saturation. ϕ is soil porosity. σ is the surface tension. p_c is capillary pressure. It was suggested that the thermodynamic-based A_{aw} may underestimate the air–water interfacial area due to not accounting for soil grain surface roughness (Brusseau, 2023a). The impact of soil grain surface roughness may be accounted for by applying a scaling factor (Zeng et al., 2021; Guo et al., 2022; Silva et al., 2022; Brusseau, 2023a). In the present study, we use a scaling factor

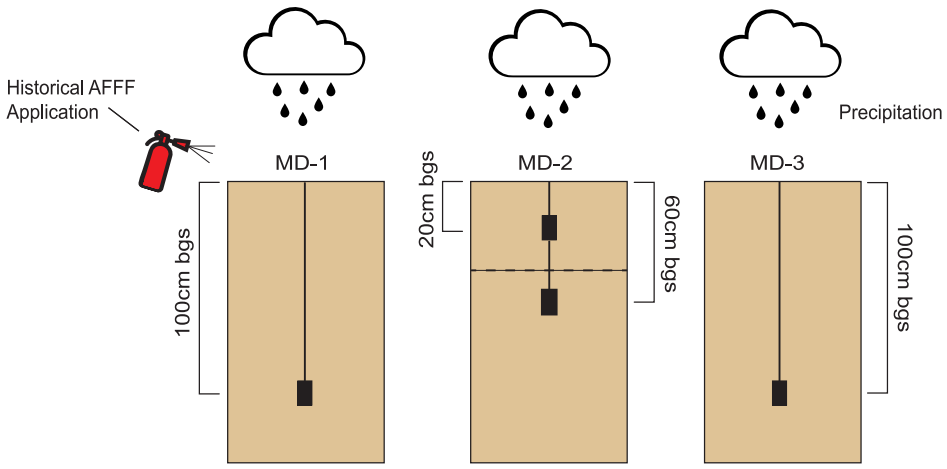

Fig. 4. Three separate 1D model domains (MD-1 to MD-3) used as three realizations of the vadose zone at the test cell. The 1D model domains of MD-1 and MD-3 assume a homogeneous vadose zone represented by the soil hydraulic parameters obtained from soil moisture probe locations 1 and 3. The model domain of MD-2 is a two-layer vadose zone (homogeneous within each layer), where the soil hydraulic parameters for the two layers were obtained from the location 2 moisture probes at depths of 20 cm and 60 cm. The dashed line represents the location of the interface between the two layers of MD-2 and was determined as a parameter from inverse modeling (Section 2.2.1). For all three model domain realizations, the top boundary is open to the atmosphere, and a free drainage condition is used at the bottom boundary.

that was empirically determined based on three sandy soils (Brusseau, 2023a),

$$SF = (-0.65S_w + 1.33)(-0.45d_{50} + 5), \quad (2)$$

where d_{50} is the soil median grain diameter (cm). As a comparison to evaluate the relevance of the scaling factor, we also conduct simulations employing the air–water interfacial area estimated by the thermodynamic-based approach without considering the soil grain surface roughness (i.e., $SF = 1$).

2.2.2. Determination of PFAS transport parameters and initial soil PFAS concentration

We determine PFAS-specific transport parameters from site-specific measurements (Schaefer et al., 2021, 2022), as well as from published data (Brusseau and Van Glubt, 2021; Nguyen et al., 2020; Guelfo and Higgins, 2013). A summary of the transport-related parameters for the four PFAS modeled in this study is presented in Table 2. Schaefer et al. (2021, 2022) each determined separate solid-phase desorption coefficients for shallow (0.03–0.9 m bgs) and deep (0.9–2.4 m bgs) soils present at the site. However, the solid-phase desorption coefficients estimated by Schaefer et al. (2021) are single-point desorption values and are likely overestimated due to the desorption not reaching equilibrium. Here, we use the solid-phase desorption coefficients reported by Schaefer et al. (2022), where the solid-phase desorption coefficients were determined by fitting the desorption data to a linear isotherm. Schaefer et al. (2022) determined that the estimated solid-phase partitioning coefficients were statistically identical for the shallow and deep intervals for both PFOA and PFOS. Therefore, we employ a single solid-phase desorption coefficient throughout the 1D model domain for each PFAS. To obtain the solid-phase desorption coefficients for PFHxS and PFBS, we scale the PFOS solid-phase desorption coefficient by the ratio of their respective normalized organic carbon-water partitioning coefficients ($K_{oc,PFHxS}/K_{oc,PFOS}$ and $K_{oc,PFBS}/K_{oc,PFOS}$) obtained from Nguyen et al. (2020), Guelfo and Higgins (2013), and ITRC (2023) (see Table S3 in the Supplementary Data (Appendix A)). Air–water interfacial adsorption coefficients (K_{aw}) for the four PFAS as a function of PFAS porewater concentration are computed by the Szyszkowski-Langmuir model (Guo et al., 2020) using parameters determined from the surface tension data measured in synthetic groundwater reported by Brusseau and Van Glubt (2021). The surface tension data were collected in an electrolyte solution with an ionic strength of 0.01 M, which matches well with the reported ionic strength of approximately 0.01 M from the porewater collected at the test cell (Schaefer et al., 2022).

For the 60-day short-term simulation scenario, we also investigate the impact of potential rate-limited solid-phase desorption on porewater concentration. We account for rate-limited solid-phase desorption by assuming that a fraction of the PFAS mass sorbed to the soil cannot be desorbed during this short simulation period, as suggested by Schaefer et al. (2022). Schaefer et al. (2022) determined the values of this fraction for both shallow and deep (i.e., $f_{RL_{shallow}}$ and $f_{RL_{deep}}$) intervals for PFOS, but for only the shallow interval for PFOA (see Table 2). Thus, we consider rate-limited desorption in the entire 1D domain for PFOS and only the shallow interval for PFOA. We do not consider rate-limited desorption for the other two shorter-chain PFAS due to unavailable data. Similarly, we do not account for rate-limited desorption from air–water interfaces for the four PFAS because we do not have any information about the model parameter values (e.g., fraction of rate-limited sites and the rate constant). Zeng et al. (2021) conducted numerical simulations of PFAS leaching in model vadose zones using parameters of rate-limited air–water interfacial adsorption obtained from miscible-displacement experiments. Their results and analysis suggest that PFAS residence time is much greater than the time scale of rate-limited air–water interfacial adsorption for both short-chain and long-chain PFAS such that rate-limited air–water interfacial adsorption has a minor impact on long-term PFAS leaching from the vadose zone. However, it is not clear to what extent rate-limited desorption may influence porewater concentrations in much shorter-term time scales (such as the 60-day period in the present study). Further investigation on the impact of potential rate-limited desorption from air–water interfaces requires additional characterization and measurements to parameterize kinetic models for air–water interfacial adsorption.

The suction lysimeters do not co-locate with the soil boring locations where soil PFAS concentrations were measured. Thus, we estimate initial total soil PFAS concentration profiles at the suction lysimeter locations by spatial interpolation of the PFAS concentration data from the soil borings (Fig. 2). This is done using the Empirical Bayesian Kriging 3D toolset in ArcGIS Pro. This geostatistical interpolation approach was selected due to the limited sample locations. Future studies should collect additional soil PFAS concentration data to further characterize the spatial heterogeneity at the test cell site. The resulting interpolated initial total soil concentration profiles for the four PFAS modeled in the present study are presented in Fig. S7 in the Supplementary Data (Appendix A).

Table 2
A summary of the transport-related parameters for the four PFAS modeled in the present study. M is the molecular weight. K_d is the solid-phase desorption coefficient. $K_{aw,max}$ is the maximum air–water interfacial adsorption coefficient computed at a porewater concentration of zero from the Langmuir isotherm, which is presented as a reference. Note that the mathematical model employs a concentration-dependent air–water interfacial adsorption coefficient directly from the Langmuir isotherm. σ_0 is the surface tension of water with no dissolved PFAS, a and b are the Szyszkowski parameters determined by fitting surface tension measurements as a function of PFAS aqueous concentration for each individual PFAS, and $f_{RL_{shallow}}$ and $f_{RL_{deep}}$ are the fraction of the soil PFAS mass exhibiting rate-limited sorption for shallow (0.03–0.9 m bgs) and deep (0.9–2.4 m bgs) soil intervals, respectively. Sources: [1] (Brusseau and Van Glubt, 2021), [2] (ITRC, 2023), [3] (Schaefer et al., 2022), [4] (Guelfo and Higgins, 2013), and [5] (Nguyen et al., 2020).

PFAS	M (g/mol)	K_d [2,3,4,5] (L/kg)	$K_{aw,max}^{[1]}$ (cm^3/cm^2)	$\sigma_0^{[1]}$ (dyn/cm)	$a^{[1]}$ ($\mu mol/cm^3$)	$b^{[1]}$ (–)	$f_{RL_{shallow}}$ [3] (–)	$f_{RL_{deep}}$ [3] (–)
PFOS	500.13	6.9	0.1184	71	0.00278	0.113	0.76	0.49
PFOA	414.07	2.2	0.0061	71.85	0.05676	0.117	0.47	–
PFHxS	400.12	0.483	0.0026	70.5	0.1547	0.141	–	–
PFBS	300.1	0.1639	1.7465×10^{-4}	71.5	1.6008	0.0953	–	–

2.2.3. Approach for model evaluation and model-based analysis

We compare the simulated porewater PFAS concentrations with samples collected by the suction lysimeters to evaluate the validity of the mathematical model during the 60-day short-term simulations. In addition to the simulations using the thermodynamic-based air–water interfacial area with and without applying the scaling factor, we conduct an additional set of simulations that do not account for the adsorption of PFAS to the air–water interfaces to evaluate the importance of air–water interfacial adsorption. To assess the impact of errors in soil moisture data on the simulated porewater PFAS concentrations, we also conduct simulations using the soil hydraulic parameters estimated with the perturbed soil moisture data described in Section 2.2.1.

Following the evaluation of simulated porewater concentrations vs. suction lysimeter data, we conduct 40-year long-term simulations to examine the primary factors controlling the long-term leaching and mass discharge of the four PFAS. Historical daily precipitation data were obtained from a nearby weather station for a period of 10 years. The 10-year data was repeated 3 times to yield a 40-year precipitation dataset. We account for evapotranspiration by multiplying the precipitation by a ratio of 0.47, which approximates the "fraction of rainfall reaching the water table" and was estimated by Schaefer et al. (2023) using the water-table fluctuation method (Gumuła-Kawęcka et al., 2022). The "not readily desorbable" fraction of the solid phase in the shorter-term desorption experiments (Schaefer et al., 2022) may behave like rate-limited desorption in the long-term simulations. Based on unpublished "rebound" experiments (i.e., sampling of porewater 2 years after the enhanced flushing experiments) conducted at the site by Schaefer and colleagues, we consider two cases of rate-limited desorption: one assumes a half-life of 6 months (i.e., $1/\alpha_s = 6$ months, where α_s is the first-order rate constant for rate-limited desorption) and the other assumes a half-life of 5 years (i.e., $1/\alpha_s = 5$ years). The rate-limited desorption is modeled by the two-site model presented in Guo et al. (2020). We compute the soil PFAS concentration profiles and the mass discharge rates to groundwater to evaluate the impact of the solid-phase rate-limited desorption. To put PFAS mass discharge to groundwater in context, we estimate the PFAS concentrations in a downgradient receptor well using the dilution factor approach suggested by US EPA (USEPA, 1996) and compare to the US EPA maximum contaminant levels (MCL) (USEPA, 2024). For computing the dilution factor, we assume a source zone area of 38 m by 12 m at the site (Weston Solutions, Inc., 2022).

In addition to using the inversely estimated soil hydraulic parameters, we also employ soil hydraulic parameters estimated from Rosetta 3 (based on the soil texture information in Table S2 in the Supplementary Data (Appendix A), but without using soil moisture data). This allows us to evaluate the value of using soil moisture data at this relatively homogeneous site. To evaluate the impact of uncertainty in the estimated parameters by Rosetta 3, we consider the upper and lower bounds of the parameters derived from Rosetta 3 (i.e., mean plus or minus two standard deviations). Because our focus is to assess the importance of air–water interfacial adsorption, we select the upper and lower bounds of the parameters such that they produce the maximum and the minimum A_{aw} (Fig. S6 in the Supplementary Data (Appendix A)). By doing so, the simulated porewater concentrations for each modeling scenario will represent the minimum and maximum possible values, respectively, based upon the available site data. The specific parameter values for each Rosetta 3 parameter set are presented in Table S5 in the Supplementary Data (Appendix A).

3. Results

3.1. Calibration and evaluation of soil hydraulic parameters

We present the observed and simulated water contents for MD-1 for both calibration and validation in Fig. 5. The results for the other two model domains (MD-2 and MD-3) are presented in Fig. S3–S5 in the Supplementary Data (Appendix A). The simulated soil water content generally agree with the observation for both the calibration and validation phases, though some notable discrepancies are observed for the shallower moisture probe (20 cm) at MD-2 and for the moisture probe (100 cm) at MD-3 during the validation phase under the simulated flushing condition (Figs. S3 and S5) in the Supplementary Data (Appendix A). The increases and decreases of the observed soil water content for the shallower probe at MD-2 are faster and more abrupt than the model simulation. This discrepancy may be caused by the presence of preferential flow pathways near the land surface that was not accounted for in the model. For the moisture probe at MD-3, the changes in the observed soil moisture content during flushing cycles are less than 0.01, which are unexpected, e.g., they are much smaller than that for the MD-1 moisture probe (approximately 0.05) at the same depth (Fig. 5). Additional data in the two locations corresponding to MD-1 and MD-3 (e.g., installation of lysimeter and soil moisture probe at another depth) may be needed to further characterize potential layered heterogeneity at the site. We have analyzed the implications of the uncertainty in soil moisture measurements as described in Section 2.2.1. The results are presented in Figs. S48–S49 and Tables S7–S8 in the Supplementary Data (Appendix A). The soil hydraulic parameters estimated from the perturbed soil moisture data are close to those calibrated using the original soil moisture data, which indicate the robustness of the inversely estimated soil hydraulic parameter values.

3.2. Evaluation of simulated porewater concentrations vs. Suction lysimeter data

We present the comparisons between the porewater concentration from the sampling lysimeter during ambient rainfall conditions and those simulated by the model for PFOS and PFOA in Figs. 6–7. The results for PFBS and PFHxS are presented in Figs. S10–S11 in the Supplementary Data (Appendix A). The model parameters were not calibrated to match the lysimeter porewater data, thus the model-data comparisons represent a direct evaluation of the model.

The average errors of the simulated porewater concentration relative to the observed values are reported in Table 4, where the definition of the relative error is presented in the caption. The results suggest

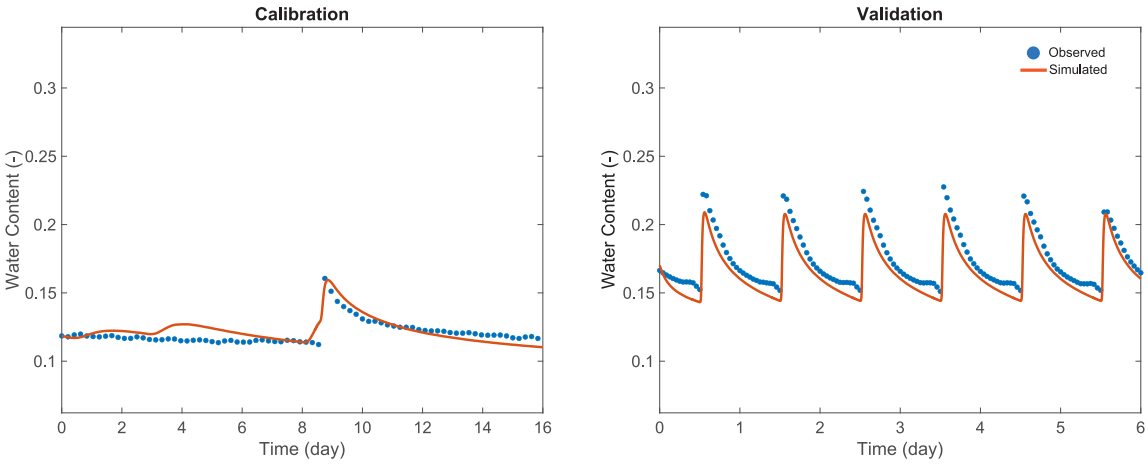

Fig. 5. Measured vs. simulated water contents during calibration (left) and validation (right) of the soil hydraulic parameters. The results for SMP-1 were presented as an example. The water content data points were coarsened for better visualization.

Table 3
Soil hydraulic parameters for the three 1D model domains determined by inverse modeling. θ_r and θ_s are the residual and saturated water contents, respectively. α, n, and L are van Genuchten–Mualem parameters for the soil water characteristics. K_{sat} is the saturated hydraulic conductivity. The model domain of MD-2 consists of two layers (top and bottom layers) separated at a depth of 47 cm.

Model domain	θ_r (−)	θ_s (−)	α (1/cm)	n (−)	K_{sat} (cm/day)	L (−)
MD-1	0.06219	0.3444	0.0265	2.774	1478	1.491
MD-2 (top layer)	0.05921	0.3471	0.0245	2.827	1478	0.1
MD-2 (bottom layer)	0.0475	0.3871	0.0494	2.866	511.5	0.966
MD-3	0.05763	0.3858	0.0256	2.773	810.2	0.788

Table 4
Relative error of simulated vs. measured PFOS, PFOA, PFHxS, and PFBS porewater concentrations at depths of 15 cm, 61 cm, 120 cm, and 150 cm. For each model depth and PFAS, the relative error is defined as the relative difference between the average simulated porewater concentration (across all three model domains and all sampling events during the 60-day period) and the average observed porewater concentration (across all sampling events during the 60-day period). The relative error is reported for both the simulations using soil hydraulic parameters estimated by (1) inverse modeling and (2) Rosetta 3 as described in Section 2.2.1, with or without accounting for air–water interfacial adsorption. When air–water interfacial adsorption is represented, A_{awi} is estimated using the thermodynamic-based method with a scaling factor. Values in parentheses are relative errors when rate-limited solid-phase desorption is accounted for.

Model depth	PFAS	Average relative error (ngL^{-1}/ngL^{-1})			
		W/ adsorption to air–water interfaces (AWIs)		W/o adsorption to AWIs	
		Inverse modeling	Rosetta 3	Inverse modeling	Rosetta 3
15 cm	PFOS	3.6 (0.03)	3.6	38.5 (8.5)	38.6
	PFOA	1.2 (0.2)	1.2	3.9 (1.6)	3.9
	PFHxS	17.4	17.2	42.3	40.9
	PFBS	5.3	4.4	4.9	3.7
61 cm	PFOS	−0.4 (−0.9)	−0.5	3.3 (0.03)	3.3
	PFOA	−0.8 (−0.9)	−0.8	−0.7 (0.8)	−0.7
	PFHxS	−0.8	−0.8	3.4	5.0
	PFBS	5.1	5.2	5.0	5.2
120 cm	PFOS	−0.5 (−0.8)	−0.6	2.9 (1.0)	3.0
	PFOA	−0.7	−0.7	−0.4	−0.4
	PFHxS	−0.7	−0.7	−0.2	−0.3
	PFBS	1.0	0.7	1.8	2.4
150 cm	PFOS	2.5 (0.8)	2.1	24.5 (12.0)	25.5
	PFOA	0.2	0.09	1.3	1.1
	PFHxS	−0.4	−0.5	0.5	0.3
	PFBS	0.5	0.5	0.9	0.9

that incorporating adsorption at air–water interfaces significantly improves the model predictions. The improvement is greater for more interfacially-active PFAS. For example, the error is reduced by more than 10 times for PFOS when accounting for the adsorption of PFOS at air–water interfaces. This indicates that air–water interfacial adsorption likely serves as a dominant process affecting the leaching of more interfacially-active PFAS in the vadose zone. Conversely, relatively small improvement is observed for the least interfacially-active PFBS. For example, the error remains unchanged for the shallower depths (15 and 61 cm) and is only reduced by approximately 50% for the deeper depths (120 and 150 cm), which suggests that the leaching of PFBS may be minimally affected by air–water interfacial adsorption. The greater impact of air–water interfacial adsorption for the interfacially-active PFAS is also reflected in the greater temporal variations of their porewater concentrations due to changes in soil wetting states. For example, the simulated PFOS porewater concentration at $z = 15$ cm changes from 121 to 457 μg/L, which is much greater than 4.5 to 8.8 μg/L for PFOA. The simulated porewater concentrations of PFOS and PFOA inversely correlate with the soil water saturation for all depths. It is notable that the temporal variation decreases at deeper depths for both PFOS

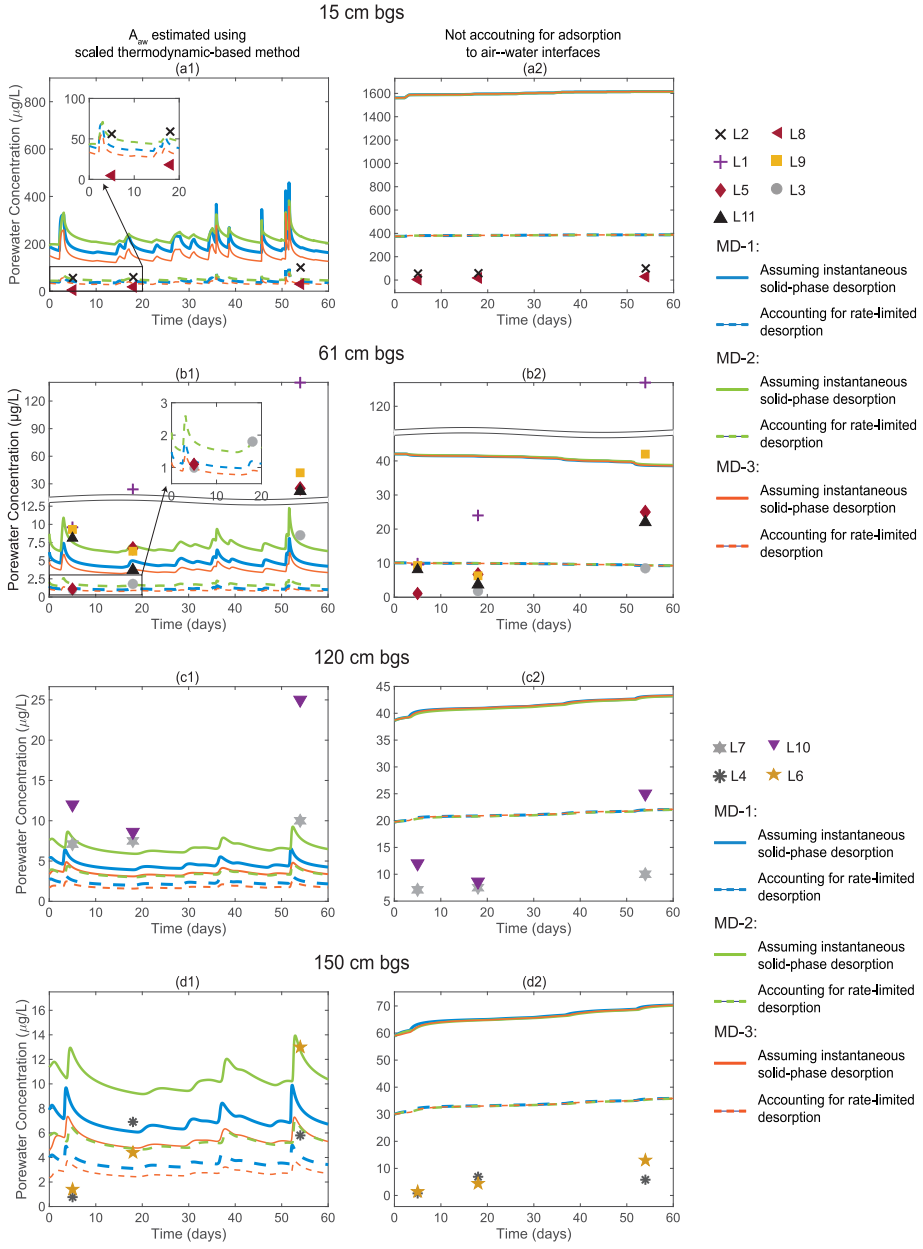

Fig. 6. Simulated vs. measured PFOS porewater concentrations at depths of 15 cm (a1–a2), 61 cm (b1–b2), 120 cm (c1–c2), and 150 cm (d1–d2), coinciding with the depths of the suction lysimeters. The simulation results include all three model domain realizations. Four cases are simulated for each model domain realization: two cases for adsorption at the air–water interface and two cases for solid-phase desorption. For adsorption at the air–water interface, one case accounts for air–water interfacial adsorption, and the other assumes no adsorption at the air–water interfaces. When air–water interfacial adsorption is represented, A_{aw} is estimated using the thermodynamic-based method with a scaling factor. For the cases pertaining to solid-phase desorption, one case accounts for rate-limited desorption by applying a fraction of the soil PFAS mass exhibiting rate-limited sorption, and the other assumes only instantaneous solid-phase desorption.

and PFOA. A closer inspection reveals that this is caused by temporal variations in soil moisture content (and hence in air–water interfacial area) decreasing over depth (Figs. S50(a1–a3)–S53(a1–a3) and Figs. S56(a1–a3)–S59(a1–a3) in the Supplementary Data (Appendix A)).

Comparing the results for A_{aw} with and without accounting for soil grain surface roughness (e.g., SF obtained from (Brusseau, 2023a) vs. $SF = 1$; the results for the latter are presented in Figs. S8–S11 in the Supplementary Data (Appendix A)) indicates that accounting for soil grain surface roughness when estimating A_{aw} leads to overall better prediction of the porewater concentrations. Representing rate-limited solid-phase desorption also generally improves the model prediction of the porewater concentrations for both PFOS and PFOA (Figs. 6–7) for the shallowest depth interval. However, PFOS sees a more significant improvement than PFOA. For example, the average error value for PFOS at $z = 15$ cm is reduced by 120 times when accounting for rate-limited solid-phase desorption while the value for PFOA is reduced by 6 times. The increased reduction in error when accounting for rate-limited solid-phase desorption in shallow soils is consistent with the experimental leaching data reported in Shea et al. (2025), who used soils from the same AFFF-impacted site.

While strong temporal variations are present in the porewater concentrations of the more interfacially-active PFOS and PFOA during the 60-day sampling period, their total soil concentrations are much more stable. Spatial profiles of all three model domains for PFOS, PFOA, PFHxS, and PFBS are presented in Figs. S12–S13, Figs. S14–S15, Figs. S16–S17, and Figs. S18–S19 in the Supplementary Data (Appendix A), respectively. As an illustrative example, we present the MD-3 spatial profiles for PFOS and PFHxS at time points which correspond to the

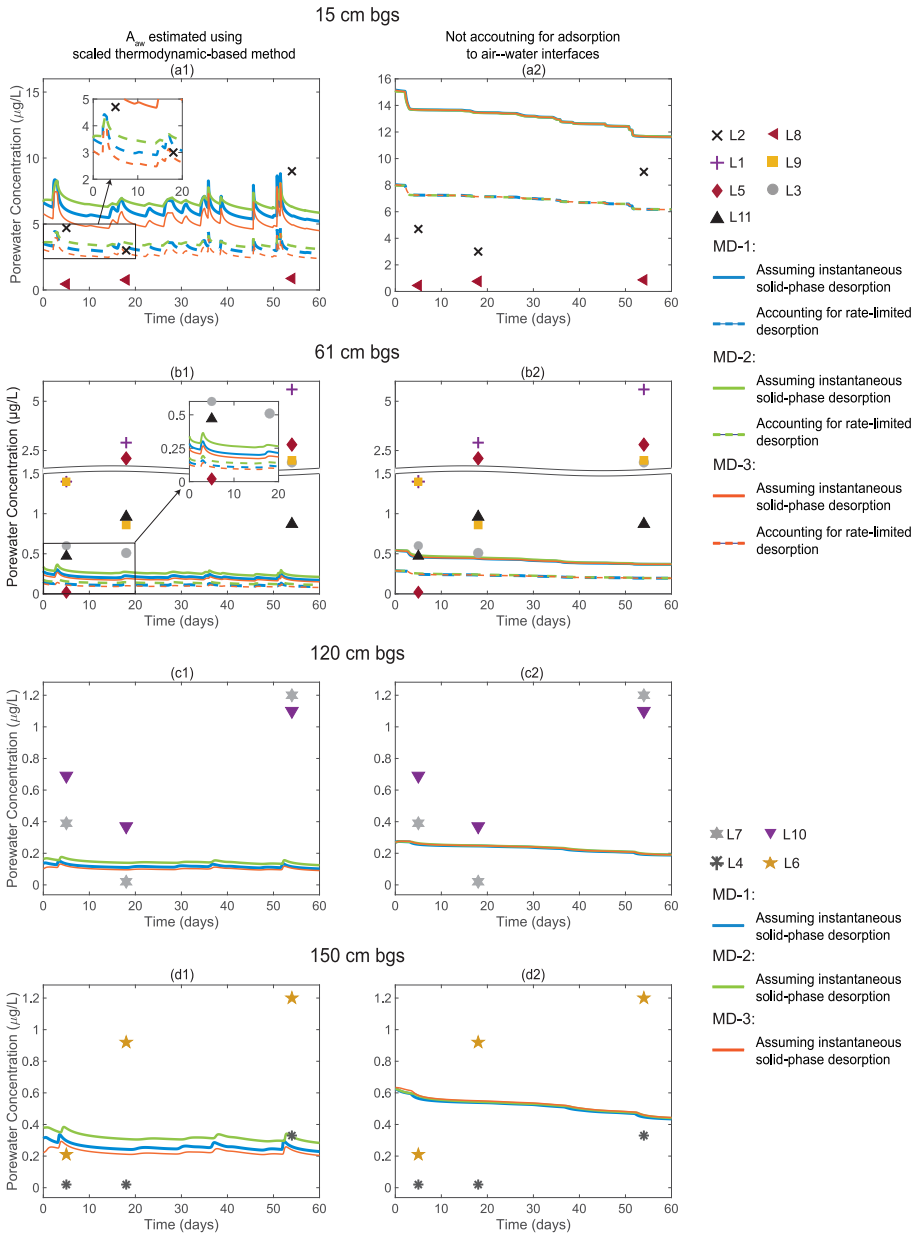

Fig. 7. Simulated vs. measured PFOA porewater concentrations at depths of 15 cm (a1–a2), 61 cm (b1–b2), 120 cm (c1–c2), and 150 cm (d1–d2), coinciding with the depths of the suction lysimeters. The simulation results include all three model domain realizations. Four cases are simulated for each model domain realization: two cases for adsorption at the air–water interface and two cases for solid-phase desorption. For adsorption at the air–water interface, one case accounts for air–water interfacial adsorption, and the other assumes no adsorption at the air–water interfaces. When air–water interfacial adsorption is represented, A_{aw} is estimated using the thermodynamic-based method with a scaling factor. For the cases pertaining to solid-phase desorption, one case accounts for rate-limited desorption by applying a fraction of the soil PFAS mass exhibiting rate-limited sorption, and the other assumes only instantaneous solid-phase desorption.

start and end of the short-term modeling scenario as well as the end of the three porewater sampling events (Figs. 8 and 9). When air–water interfacial adsorption is represented (Fig. 8(a1–a4)), the spatial profiles for PFOS indicate minimal downward migration during the period of 60 days. However, the porewater concentration and solid-phase adsorption profiles do vary among the four time points, which are caused by the redistribution of PFOS mass in porewater, solid-phase adsorption, and at the air–water interfaces, due to changes in water saturation and air–water interfacial area. The time series of porewater concentration of PFOS, air–water interfacial area, and water saturation at depths of 15 cm, 61 cm, 120 cm, and 150 cm (Figs. S50(a1–a3)–S53(a1–a3) in the Supplementary Data (Appendix A)) show strong positive correlation between porewater concentration and water saturation (and strong negative correlation with air–water interfacial area) with no apparent effective change in PFOS soil concentration. During the 60 days, approximately 1%, 12%, and 87% of the PFOS mass is in the porewater, adsorbed solid phase, and adsorbed to the air–water interface, respectively. Visible downward migration is observed over the period of 60 days when air–water interfacial adsorption is turned off (Fig. 8(b1–b4)). In this case, the changes in the porewater concentration are primarily caused by changes in the total soil concentration (i.e., downward migration) rather than by mass redistribution.

Conversely, the spatial profiles for PFHxS (Fig. 9(a1–a4)) suggest notable downward migration even when air–water interfacial adsorption is present. Approximately 28%, 22%, and 50% of the PFHxS mass is in the porewater, solid-phase adsorption, and air–water interfacial adsorption, respectively. A closer inspection reveals that some of the

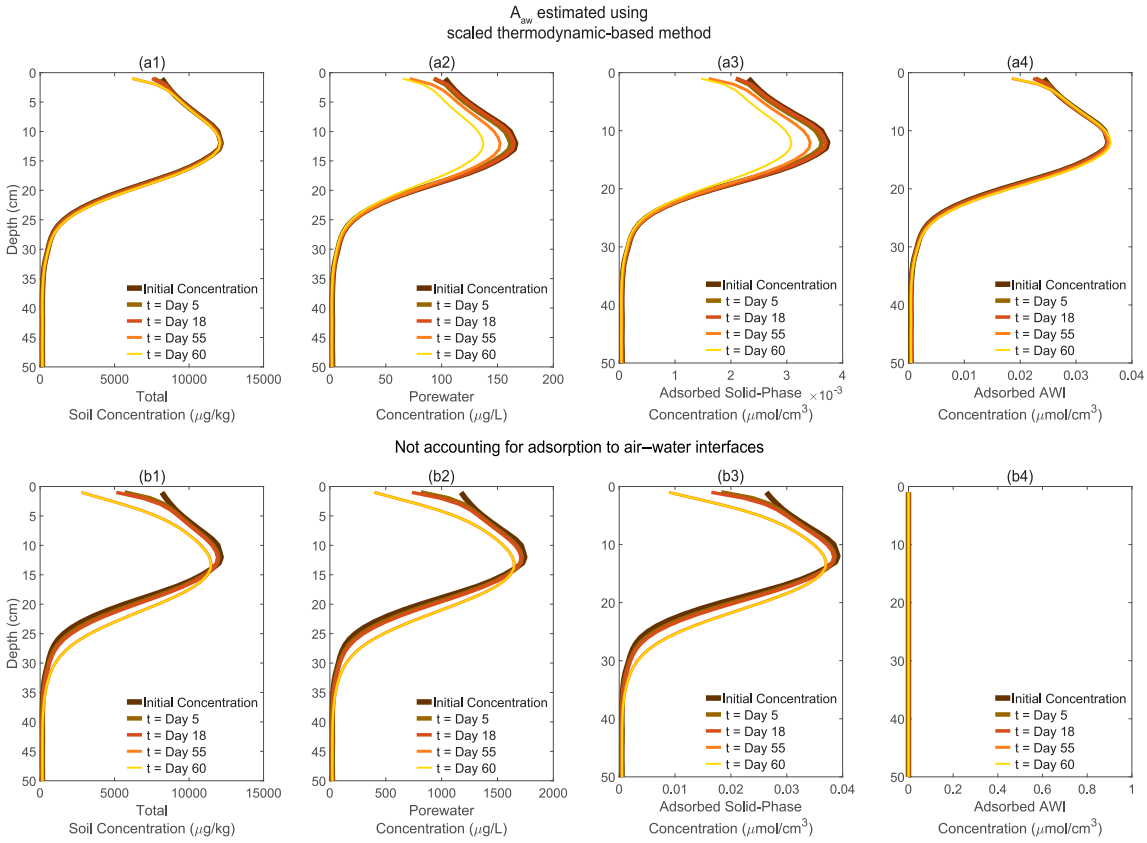

Fig. 8. Simulated PFOS concentration profiles for model domain MD-3 during evaluation of simulations vs. suction lysimeter data. Profiles are plotted for total soil concentration (a1–b1), porewater concentration (a2–b2), adsorbed solid-phase concentration (a3–b3), and adsorbed air–water interfacial concentration (a4–b4). Profiles are plotted at time steps coinciding with the: initialization of the model domain, conclusion of the three separate porewater lysimeter sampling events, and conclusion of the simulation. Two cases are simulated for each model domain realization. One accounts for air–water interfacial adsorption (a1–a4), and the other assumes no adsorption at the air–water interfaces (b1–b4). When air–water interfacial adsorption is represented, A_{aw} is estimated using the thermodynamic-based method with a scaling factor.

changes in the porewater among the four time points are caused by mass redistribution among the three phases, resulting from changes in water saturation and air–water interfacial area. As expected, turning off air–water interfacial adsorption leads to much greater downward migration (Fig. 9(b1–b4)).

The above results indicate that porewater lysimeter data for the more interfacially-active PFAS, like PFOS, collected over relatively short time intervals under different wetting conditions reflect the mass distributions among the three phases, rather than representing their downward leaching. This insight can be used to constrain the estimated air–water interfacial area using the lysimeter porewater concentration combined with soil moisture data, which is discussed in Section 4.

We analyze the impact of soil hydraulic parameter uncertainties on the predicted porewater concentrations by comparing simulations using soil hydraulic parameters calibrated to the original soil moisture data and the perturbed soil moisture data. We present comparisons between these simulations for PFOS and PFOA in Figs. S50–S53 and Figs. S56–S59 in the Supplementary Data (Appendix 3), respectively. The simulated porewater concentrations using the three sets of hydraulic parameters are very close. The deviations are between −24.03% and 18.92% for PFOS and −14.42% and 11.3% for PFOA. These results suggest that potential uncertainties in the soil moisture measurements appear to have a relatively minor impact on simulated PFOS and PFOA porewater concentrations.

The simulated porewater concentrations using the Rosetta 3 parameters vs. suction lysimeter data are presented in Fig. S44 and Fig. S45 in the Supplementary Data (Appendix A) for PFOS and PFOA, respectively. Comparing the PFOS simulations results using the Rosetta 3 parameters in Fig. S44 with those using the inversely modeled parameters in Fig. S8, the upper and lower ranges of porewater concentrations simulated by the Rosetta 3 parameters bracket the range of concentrations simulated by the inversely modeled parameters. In addition, there is little difference between the porewater concentrations estimated using the average Rosetta 3 parameter set and the concentrations simulated by the inversely modeled parameters. This is consistent with the average relative errors in Table 4. Similar behaviors are observed for PFOA. These results indicate that for this specific site, the use of parameters derived from Rosetta 3 using soil texture may be equally applicable to simulating PFAS leaching and mass discharge to groundwater compared to using the parameters calibrated to soil moisture data. But, this finding may be specific to this relatively homogeneous site and may not be the case for more heterogeneous or otherwise complicated sites.

3.3. Model-based analysis of long-term leaching and mass discharge

We analyze the 40-year simulations to examine the primary factors controlling long-term leaching of PFAS in the vadose zone and mass discharge to groundwater at the site. Descriptions of the model setup and parametrization are presented in Section 2.2.2. We computed the mass remaining in the vadose zone and temporal mass discharge rates for each PFAS. The results for PFOS and PFHxS are presented in Fig. 10 for illustration. The results for the other two PFAS, PFOA and PFBS, are presented in Figs. S21 and S22 in the Supplementary Data (Appendix A), respectively. First, while the hydraulic properties of the three model domains are different, the difference among them is relatively small. This is consistent with the porewater concentration analysis in Section 3.2 and the field observation by Schaefer et al.

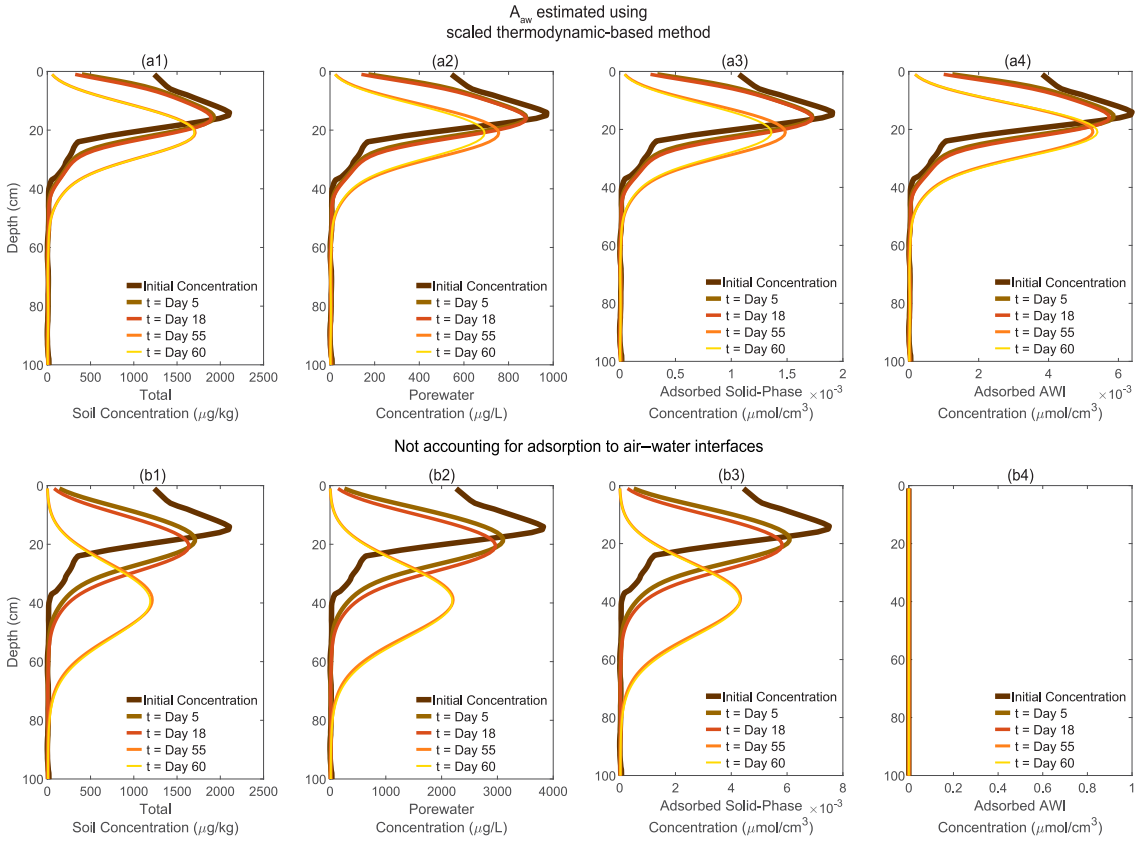

Fig. 9. Simulated PFHxS concentration profiles for model domain MD-3 during evaluation of simulations vs. suction lysimeter data. Profiles are plotted for total soil concentration (a1–b1), porewater concentration (a2–b2), adsorbed solid-phase concentration (a3–b3), and adsorbed air–water interfacial concentration (a4–b4). Profiles are plotted at time steps coinciding with the: initialization of the model domain, conclusion of the three separate porewater lysimeter sampling events, and conclusion of the simulation. Two cases are simulated for each model domain realization. One accounts for air–water interfacial adsorption (a1–a4), and the other assumes no adsorption at the air–water interfaces (b1–b4). When air–water interfacial adsorption is represented, A_{aw} is estimated using the thermodynamic-based method with a scaling factor.

(2022, 2023) that the site is relatively homogeneous. Second, PFAS with a greater interfacial activity are more strongly retained in the vadose zone. For example, more than 95% of the total PFOS mass still remains in the vadose zone even after 40 years of leaching. Conversely, the leaching for the other three PFAS is much faster. 99% of the mass in the vadose zone has been discharged to groundwater after 37 years for PFOA, 15 years for PFHxS, and 3 years for PFBS.

We have also estimated the groundwater concentration at a downgradient receptor well as a function of time using the US EPA dilution approach (Fig. S24(a1–d1) in the Supplementary Data (Appendix A)). Since the majority of the PFOS mass remains in the vadose zone, the estimated groundwater concentrations in the receptor well stay at a relatively low level (between 5.44×10^{-3} to 27.24×10^{-3} μg/L) during the 40 years of simulation. Despite that the PFOS concentrations still exceed the US EPA drinking water MCL of 0.004 μg/L set for PFOS. The estimated receptor groundwater concentrations all reach the peak within the 40 years of simulation. The maximum concentrations for PFOA, PFHxS, and PFBS are 5.095×10^{-3}, 892.84×10^{-3}, and 6.19×10^{-2} μg/L, respectively. The maximum concentrations for PFOA and PFHxS exceed their US EPA drinking water MCL of 0.004 μg/L and 0.01 μg/L, respectively.

The spatial concentration profiles further illustrate the different leaching behaviors among the four PFAS. The results for PFOS and PFHxS are presented in Fig. 11. The spatial concentration profiles for PFOA and PFBS are presented in Figs. S26 and S28 in the Supplementary Data (Appendix A), respectively. The center of the PFOS plume in the vadose zone has only migrated 30 cm over the 40 years of simulation. This is consistent with the field observation at the site where the center of the PFOS plume measured in 2019 was only 12 cm below the land surface 23 years after the last known AFFF application at the site. However, the model simulations for the other three less interfacially-active PFAS appear to deviate from the field data. While the model simulations indicate that most of their mass has been discharged to groundwater after a few decades, the soil concentrations measured in 2019 (23 years after the last known AFFF application at the site) showed that most of their mass still remains in the shallow soil near the land surface. This discrepancy could be due to the prior simulations not accounting for rate-limited desorption, which we discuss below.

The rate-limited desorption sensitivity analysis for PFOS (Fig. S29) suggests that rate-limited solid-phase desorption (assuming a half-life (i.e., $1/\alpha_s$) of 6 months or 5 years) has a minimal impact on PFOS leaching. This is expected because the half-life (6 months or 5 years) for rate-limited desorption is small relative to the residence time of PFOS in the vadose zone. For the less interfacially-active PFOA, PFHxS, and PFBS (Figs. S32, S35, and S38 in the Supplementary Data (Appendix A)), rate-limited desorption has a greater impact and reduces their leaching rates in the vadose zone (especially with the greater half-life of 5 years). This reduction is more notable for the less interfacially-active shorter-chain PFAS due to their shorter residence times in the vadose zone. The above analysis indicates that the presence of rate-limited desorption might be a potential cause of the overestimated leaching for the less interfacially-active PFAS when assuming instantaneous desorption. This issue is further discussed in Section 4.

Comparing the simulation results with and without accounting for the adsorption at air–water interfaces indicates that the adsorption to the air–water interface plays an important role in controlling the

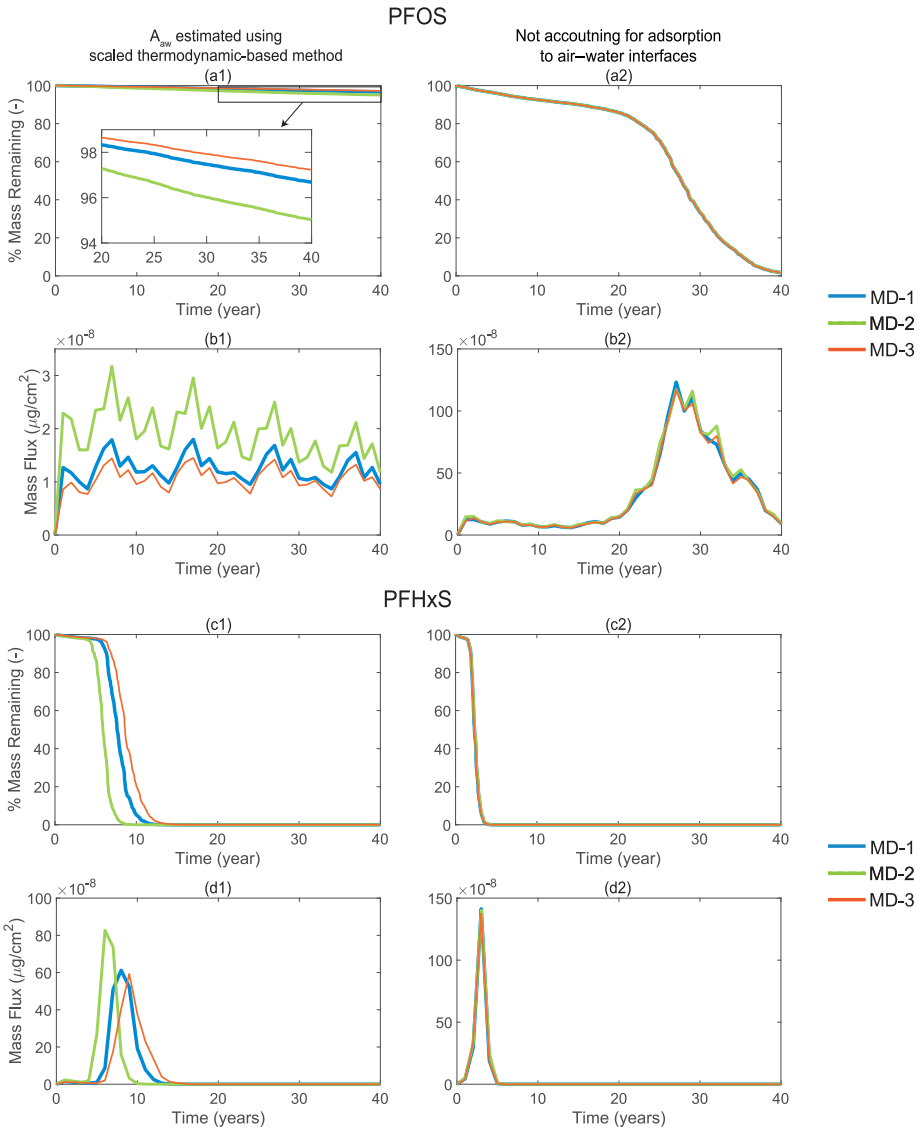

Fig. 10. Simulated PFOS and PFHxS: percent mass remaining in the vadose zone and mass flux from the vadose zone to groundwater during model-based analysis of long-term leaching and mass discharge. The simulation results include all three model domain realizations. Two cases are simulated for each model domain realization. One accounts for air–water interfacial adsorption (a1–d1), and the other assumes no adsorption at the air–water interfaces (a2–d2). When air–water interfacial adsorption is represented, A_{aw} is estimated using the thermodynamic-based method with a scaling factor.

long-term leaching and mass discharge of the more interfacially-active PFOS (Figs. 10 and 11). Without air–water interfacial adsorption, the leaching of PFOS is much faster, and almost all of the PFOS mass in the vadose zone has been discharged to groundwater at the end of the 40 years. However, air–water interfacial adsorption appears to be much less important for the other three less interfacially-active PFAS, indicated by the relatively small difference between the simulated leaching with and without accounting for air–water interfacial adsorption. These observations are consistent with the analysis of the porewater concentrations in 3.2.

As expected from the porewater concentration simulations in Section 3.2, the long-term simulations using the soil hydraulic parameters generated by Rosetta 3 (Table S5) are generally similar to those simulated using the inversely estimated soil hydraulic parameters (Figs.S46 and S47 for the results for PFOS and PFOA, respectively). This indicates that soil hydraulic parameters estimated from Rosetta 3 using soil texture may be used as a first estimate for a screening-type analysis when no detailed datasets are available, especially at relatively homogeneous sites like the one in our study.

4. Discussion

The porewater concentration analysis (Sections Section 3.2) and long-term simulations (Section 3.3) both suggest that air–water interfacial adsorption is an important process that needs to be represented when modeling the leaching of PFAS in the vadose zone and mass discharge to groundwater, especially for the more interfacially-active PFOS. As discussed in Section 3.3, the minimal downward migration of PFOS during the 40-year simulation period is consistent with the strong retention observed at the site (Fig. 2). However, while the agreement between the model-simulated and measured porewater concentrations for PFOA, PFHxS, and PFBS is similar to that for PFOS, their long-term model simulations generally predict much faster leaching than the field-observed data, especially for the shorter-chain PFHxS and PFBS. It is notable that the soil concentration profiles for PFOS, PFOA, PFHxS, and PFBS in Fig. 2 do not appear to exhibit differential mobility at the site, contrary to many field observations at other sites (Brusseau et al., 2020; Bigler et al., 2024). The reason behind this phenomenon is unclear. We have analyzed the potential impact of air–water interfacial adsorption coefficient uncertainties on the simulated PFAS leaching by

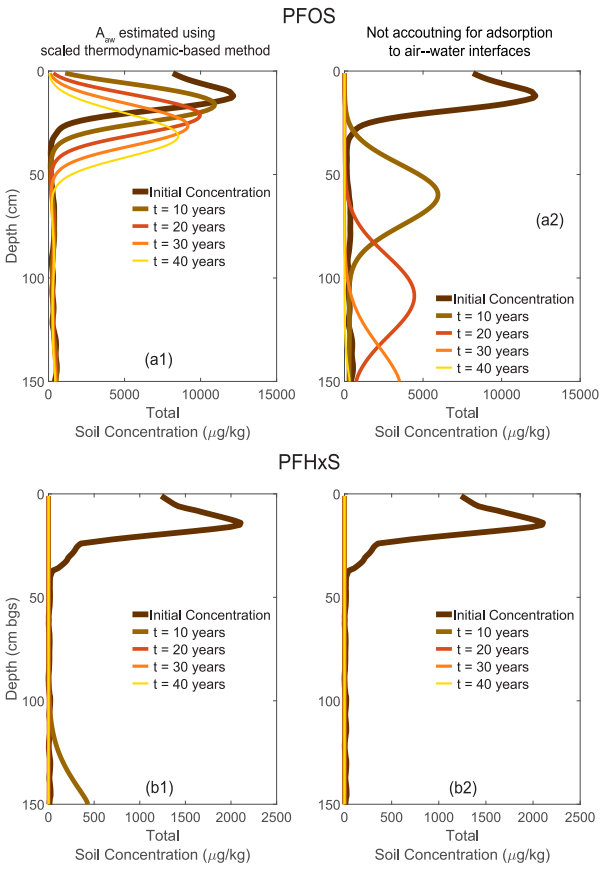

Fig. 11. Simulated PFOS (a1–a2) and PFHxS (b1–b2) total soil concentration profiles during model-based analysis of long-term leaching and mass discharge. Simulation results include all three model domain realizations. Two cases are simulated for each model domain realization. One accounts for air–water interfacial adsorption (a1–b1), and the other assumes no adsorption at the air–water interfaces (a2–b2). When air–water interfacial adsorption is represented, A_{aw} is estimated using the thermodynamic-based method with a scaling factor.

perturbing the air–water interfacial adsorption coefficient by a factor of 0.5 and 2 (See Section S9 in the Supplementary Data (Appendix A)). As expected, PFAS leaching increases for a smaller air–water interfacial adsorption coefficient, but the sensitivity decreases with chain length (i.e., interfacial activity). For example, the leaching of PFBS is almost insensitive to changes to the air–water interfacial adsorption coefficient. This suggests that uncertainties in the air–water interfacial coefficients may not explain the observed overestimated leaching for the shorter-chain PFAS.

Furthermore, we have analyzed the potential impact of solid-phase desorption coefficient uncertainties on the simulated leaching of the shorter-chain PFAS. We represent the uncertainties of K_d by considering uncertainties in the K_{oc} values compiled in Brusseau (2024) (See Section S10 in the Supplementary Data (Appendix A)). Using the mean K_{oc}, and one standard deviation greater and smaller than the mean, we obtained mean, greater and smaller estimates of K_d for PFHxS and PFBS. The greater estimates of K_d lead to much greater retention of PFHxS and PFBS in the vadose zone than that of the mean K_d (Figures S80–81 and S84–85), which is more consistent with the soil concentration profiles observed in the field. This indicates that uncertainties in solid-phase desorption coefficients may partly explain the underestimated retention of PFHxS and PFBS in the model simulations.

Another potential explanation could be that precursors retained in the shallow soil continuously generate PFOA, PFHxS, and PFBS. Retention of precursors in shallow soil in the source zone and in groundwater near the source zone has been observed at a range of AFFF-impacted sites decades after the last known AFFF release (Houtz et al., 2013; Adamson et al., 2020; Nickerson et al., 2020, 2021; Liu et al., 2021; Ruyle et al., 2023). However, additional site investigation is required to examine the extent to which precursor transformation impacts the long-term leaching of perfluoroalkyl acids (PFAAs) at the present test cell site.

Rate-limited desorption directly affects the sampled porewater concentrations for PFOS and PFOA, particularly for the shallowest depth interval. The analysis in Section 3.2 indicates that accounting for this process greatly reduces the discrepancies between the simulated and measured porewater concentrations in shallow soil. This highlights the importance of characterizing the desorption kinetics of PFAS using field-collected soil samples for interpreting porewater concentrations obtained from suction lysimeters. It is likely that the appeared "not readily desorbable" solid-phase adsorbed PFAS observed in the desorption experiments in Schaefer et al. (2021, 2022) may exhibit as rate-limited desorption if the experiments were conducted for a longer period of time. Longer-term experiments (e.g., batch experiments) may be needed to characterize the timescale of rate-limited desorption. The simulations in Section 3.3 accounting for rate-limited desorption suggest that long-term leaching of the shorter-chain PFAS could be controlled by rate-limited desorption when kinetic desorption involves longer time scales, e.g., 6 months to 5 years.

As discussed in Section 2, the air–water interfacial area is one of the parameters that may involve significant uncertainties. Given that air–water interfacial adsorption acts as a primary retention process, any uncertainty in the estimated air–water interfacial area will be propagated to the predicted PFAS leaching and mass discharge to groundwater. As discussed in Section 3.2, given that the soil concentration of the more interfacially-active longer-chain PFAS (e.g., PFOS) remains almost unchanged during the 60-day sampling period, the suction lysimeter porewater concentration data, together with other datasets, may be used to constrain the estimation of the air–water interfacial area. If the soil concentration remains unchanged, the change of porewater concentration is entirely caused by the redistribution of mass among the three phases (aqueous, solid-phase, and air–water interfaces)

$$C_{\text{soil}} = \theta C_{aq} + \rho_b K_d C_{aq} + A_{aw} K_{aw} C_{aq}, \tag{3}$$

where C_{soil} is the soil PFAS concentration. θ is the water content. C_{aq} is the aqueous PFAS concentration. ρ_b is the soil bulk density. K_{aw} is the air–water interfacial adsorption coefficient. With the porewater concentration from the suction lysimeters and estimated values for the other parameters, we can then estimate A_{aw} as

$$A_{aw} = \frac{C_{\text{soil}} - \theta C_{aq} - \rho_b K_d C_{aq}}{K_{aw} C_{aq}}. \tag{4}$$

Assuming that the thermodynamic-based A_{aw} provides a reasonable estimate on the dependence of A_{aw} on water saturation, then our goal is to estimate the microscale surface roughness scaling factor SF (Eq. (2)). As an illustration of the approach described above, we use the porewater concentration data of PFOS and PFOA to calibrate the roughness scaling factor SF for estimating A_{aw}. Detailed description and application of this method for PFOS and PFOA simulation results are presented in Section S6 of the Supporting Information. Note that C_{soil} in Eq. (4) should subtract the "not readily desorbable" fraction that cannot be desorbed during the sampling period. The estimated scaling factors obtained from the PFOS and PFOA porewater concentration data are presented in Table S4.

Comparison between the simulated (using the A_{aw} with the newly estimated scaling factor SF) and measured porewater concentrations for PFOS and PFOA are shown in Figs. S41-S42, respectively. As expected, the agreement with the measured porewater concentrations is better than that directly using the predicted SF from Eq. (2). The estimated SF values for PFOS and PFOA are consistent, with a difference generally less than a factor of 2. The estimated SF values

exhibit significant variations over depths. For example, the SF values are greater than 15 at the depths of 15 cm and 150 cm, but are less than 4.2 at 61 cm and 120 cm. As a comparison, the SF predicted by Eq. (2) is approximately 5.0–5.5 (depending on the water saturation). This indicates that the SF constrained by lysimeter porewater concentration data could greatly improve the estimated A_{aw} at the depths of 15 cm and 150 cm. However, we note that because Eq. (2) was derived from air–water interfacial area datasets obtained for sandy soils (Brusseau, 2023a), it is expected that it may introduce greater uncertainties when applied to other types of finer-grained soils with greater microscale surface roughnesses (e.g., soils with greater clay or silt fractions). Under those conditions, constraining A_{aw} using the lysimeter porewater concentration data will be especially valuable.

Finally, all the model simulations in the present study assume a 1D representation of the vadose zone, which does not account for the potential existence of lateral heterogeneities and preferential flow pathways. Prior multidimensional modeling studies (Zeng and Guo, 2021, 2023) have demonstrated that spatial heterogeneities can accelerate PFAS leaching in the vadose zone due to reduced air–water interfacial area (and hence reduced air–water interfacial adsorption) along the preferential flow pathways. While 1D simulations appear to work reasonably well for the relatively homogeneous test cell site in the present study, multidimensional models may be required to capture the impact of heterogeneity on PFAS leaching at other more complex PFAS-contaminated sites.

5. Conclusions

We have combined field data sets collected at an AFFF-impacted site (Schaefer et al., 2022, 2023) with mathematical models (Guo et al., 2020) to quantify PFAS leaching and mass discharge in the vadose zone. We have demonstrated that representing air–water interfacial adsorption is critical for accurately simulating PFAS porewater concentrations sampled by suction lysimeters at the site and for quantifying PFAS leaching in the vadose zone and mass discharge to groundwater, especially for the more interfacially-active PFAS such as PFOS and PFOA. The good agreement between the predicted and measured porewater concentrations represents a direct validation of the mathematical model that accounts for PFAS-specific retention and transport processes.

Over a relatively short time interval during lysimeter sampling (e.g., 2 months in the present study), the modeling analysis suggests that minimal spatial migration of PFOS and PFOA had occurred and the variations observed in the porewater concentration collected at different sampling events and different depths primarily reflect the redistribution of PFAS mass among porewater, solid-phase adsorption, and mass adsorbed at the air–water interface. The redistribution of mass is driven by dynamic changes in soil moisture content and air–water interfacial area. Based on this insight, one can combine the lysimeter porewater concentration and soil moisture data to estimate and constrain the air–water interfacial area, which has been considered one of the parameters involving the greatest uncertainties. Our results also suggest that, due to rate-limited solid-phase desorption, some significant fraction of the solid-phase adsorption may not desorb during a relatively short sampling time interval. This is an important factor that needs to be characterized and quantified to accurately interpret the porewater concentrations sampled using suction lysimeters.

Analysis of the 40-year long-term simulations suggests that most of the PFOS mass remains in the shallow soil (the center of the mass has only migrated to approximately 30 cm below the land surface). This is in agreement with the minimal downward migration observed in the soil PFOS concentrations measured 23 years after the last AFFF application. However, the model simulations assuming instantaneous solid-phase desorption predict much faster leaching for PFOA, PFHxS, and PFBS than the field observations. The discrepancies may be caused by the generation of these three PFAS from precursor transformation and/or rate-limited desorption that reduces leaching. Additional simulations accounting for rate-limited desorption indicate that rate-limited desorption (with a half-life of 6 months or 5 years) can reduce the leaching of PFOA, PFHxS, and PFBS. Another possibility is that the solid-phase desorption coefficients for these PFAS may be underestimated. Differentiating the causes by the different mechanisms will require more comprehensive investigations involving both additional data collection and model parametrization (e.g., characterizing and representing solid-phase desorption kinetics and precursor transformation).

CRediT authorship contribution statement

Ryan Russell: Writing – original draft, Visualization, Software, Methodology, Investigation, Formal analysis, Data curation. **Bo Guo:** Writing – review & editing, Supervision, Software, Project administration, Methodology, Investigation, Funding acquisition, Formal analysis, Data curation, Conceptualization. **Jicai Zeng:** Writing – review & editing, Software, Methodology. **Mark L. Brusseau:** Writing – review & editing, Methodology, Funding acquisition. **Charles E. Schaefer:** Writing – review & editing, Methodology, Data curation. **Stefanie Shea:** Writing – review & editing, Data curation. **Christopher P. Higgins:** Writing – review & editing, Data curation. **Ty P.A. Ferre:** Writing – review & editing, Methodology.

Declaration of competing interest

The authors declare that they have no known competing financial interests or personal relationships that could have appeared to influence the work reported in this paper.

Acknowledgments

This work was in part supported by the Environmental Security Technology Certification Program, United States (ESTCP Project ER21-5041) and National Science Foundation, United States (2237015).

Appendix A. Supplementary data

Supplementary material related to this article can be found online at https://doi.org/10.1016/j.watres.2025.124063.

Data availability

All data used in the study have been reported in the manuscript and supporting information.

References

Adamson, D.T., Nickerson, A., Kulkarni, P.R., Higgins, C.P., Popovic, J., Field, J., Rodowa, A., Newell, C., DeBlanc, P., Kornuc, J.J., 2020. Mass-based, field-scale demonstration of PFAS retention within AFFF-Associated Source Areas. Environ. Sci. Technol. 54 (24), 15768–15777.

Anderson, R.H., 2021. The case for direct measures of soil-to-groundwater contaminant mass discharge at AFFF-impacted sites. Environ. Sci. Technol. 55 (10), 6580–6583.

Anderson, R.H., Feild, J.B., Dieffenbach-Carle, H., Elsharnouby, O., Krebs, R.K., 2022. Assessment of PFAS in collocated soil and porewater samples at an AFFF-impacted source zone: Field-scale validation of suction lysimeters. Chemosphere 308, 136247.

Arshadi, M., Garza-Rubalcava, U., Guedes, A., Cápiro, N.L., Pennell, K.D., Christ, J., Abriola, L.M., 2024. Modeling 1-D aqueous film forming foam transport through the vadose zone under realistic site and release conditions. Sci. Total Environ. 919, 170566.

Bigler, M.C., Brusseau, M.L., Guo, B., Jones, S.L., Pritchard, J.C., Higgins, C.P., Hatton, J., 2024. High-resolution depth-discrete analysis of PFAS distribution and leaching for a vadose-zone source at an AFFF-impacted site. Environ. Sci. Technol.

Brusseau, M.L., 2023a. Determining air–water interfacial areas for the retention and transport of PFAS and other interfacially active solutes in unsaturated porous media. Sci. Total Environ. 163730.

Brusseau, M.L., 2023b. QSPR-based prediction of air-water interfacial adsorption coefficients for nonionic PFAS with large headgroups. Chemosphere 340, 139960.
Brusseau, M.L., 2024. Field versus laboratory measurements of PFAS sorption by soils and sediments. J. Hazard. Mater. Adv. 16, 100508.
Brusseau, M.L., Anderson, R.H., Guo, B., 2020. PFAS concentrations in soils: Background levels versus contaminated sites. Sci. Total Environ. 740, 140017.
Brusseau, M., Guo, B., 2022. PFAS concentrations in soil versus soil porewater: Mass distributions and the impact of adsorption at air-water interfaces. Chemosphere 302, 134938.
Brusseau, M.L., Guo, B., Huang, D., Yan, N., Lyu, Y., 2021. Ideal versus nonideal transport of PFAS in unsaturated porous media. Water Res. 202, 117405.
Brusseau, M.L., Khan, N., Wang, Y., Yan, N., van Glubt, S., Carroll, K.C., 2019. Nonideal transport and extended elution tailing of PFOS in soil. Environ. Sci. Technol.
Brusseau, M.L., Van Glubt, S., 2021. The influence of molecular structure on PFAS adsorption at air–water interfaces in electrolyte solutions. Chemosphere 281, 130829.
Devices, D.-T., 2016. User Manual for the Profile Probe Type PR2. Delta-T Devices Ltd., Cambridge, UK.
Garza-Rubalcava, U., Klevan, C., Pennell, K.D., Abriola, L.M., 2024. Transport and competitive interfacial adsorption of PFOA and PFOS in unsaturated porous media: experiments and modeling. Water Res. 122728.
Guelfo, J.L., Higgins, C.P., 2013. Subsurface transport potential of perfluoroalkyl acids at aqueous film-forming foam (AFFF)-impacted sites. Environ. Sci. Technol. 47 (9), 4164–4171.
Gumuła-Kawęcka, A., Jaworska-Szulc, B., Szymkiewicz, A., Gorczewska-Langner, W., Pruszkowska-Caceres, M., Angulo-Jaramillo, R., Šimůnek, J., 2022. Estimation of groundwater recharge in a shallow sandy aquifer using unsaturated zone modeling and water table fluctuation method. J. Hydrol. 605, 127283.
Guo, B., Zeng, J., Brusseau, M.L., 2020. A mathematical model for the release, transport, and retention of per-and polyfluoroalkyl substances (PFAS) in the vadose zone. Water Resour. Res. 56 (2), e2019WR026667.
Guo, B., Zeng, J., Brusseau, M.L., Zhang, Y., 2022. A screening model for quantifying PFAS leaching in the vadose zone and mass discharge to groundwater. Adv. Water Resour. 160, 104102.
Houtz, E.F., Higgins, C.P., Field, J.A., Sedlak, D.L., 2013. Persistence of perfluoroalkyl acid precursors in AFFF-impacted groundwater and soil. Environ. Sci. Technol. 47 (15), 8187–8195.
ITRC, 2023. History and Use of Per- and Polyfluoroalkyl Substances (PFAS) Found in the Environment. Technical Report, The Interstate Technology and Regulatory Council (ITRC).
Leverett, M., 1941. Capillary behavior in porous solids. Trans. AIME 142 (01), 152–169.
Liao, S., Arshadi, M., Woodcock, M.J., Saleeba, Z.S., Pinchbeck, D., Liu, C., Cápiro, N.L., Abriola, L.M., Pennell, K.D., 2022. Influence of residual nonaqueous-phase liquids (NAPLs) on the transport and retention of perfluoroalkyl substances. Environ. Sci. Technol. 56 (12), 7976–7985.
Liu, M., Munoz, G., Vo Duy, S., Sauvé, S., Liu, J., 2021. Per-and polyfluoroalkyl substances in contaminated soil and groundwater at airports: a Canadian case study. Environ. Sci. Technol. 56 (2), 885–895.
Morrow, N.R., 1970. Physics and thermodynamics of capillary action in porous media. Ind. Eng. Chem. 62 (6), 32–56.
Nguyen, T.M.H., Braunig, J., Thompson, K., Thompson, J., Kabiri, S., Navarro, D.A., Kookana, R.S., Grimison, C., Barnes, C.M., Higgins, C.P., 2020. Influences of chemical properties, soil properties, and solution pH on soil–water partitioning coefficients of per- and polyfluoroalkyl substances (PFASs). Environ. Sci. Technol. 54 (24), 15883–15892.
Nickerson, A., Maizel, A.C., Kulkarni, P.R., Adamson, D.T., Kornuc, J.J., Higgins, C.P., 2020. Enhanced extraction of AFFF-associated PFASs from source zone soils. Environ. Sci. Technol. 54 (8), 4952–4962.
Nickerson, A., Rodowa, A.E., Adamson, D.T., Field, J.A., Kulkarni, P.R., Kornuc, J.J., Higgins, C.P., 2021. Spatial trends of anionic, zwitterionic, and cationic PFASs at an AFFF-impacted site. Environ. Sci. Technol. 55 (1), 313–323.
Quinnan, J., Rossi, M., Curry, P., Lupo, M., Miller, M., Korb, H., Orth, C., Hasbrouck, K., 2021. Application of PFAS-mobile lab to support adaptive characterization and flux-based conceptual site models at AFFF releases. Remediat. J. 31 (3), 7–26.
Ruyle, B.J., Thackray, C.P., Butt, C.M., LeBlanc, D.R., Tokranov, A.K., Vecitis, C.D., Sunderland, E.M., 2023. Centurial persistence of forever chemicals at military fire training sites. Environ. Sci. Technol. 57 (21), 8096–8106.
Schaefer, C.E., Culina, V., Nguyen, D., Field, J., 2019. Uptake of poly- and perfluoroalkyl substances at the air–water interface. Environ. Sci. Technol. 53 (21), 12442–12448.
Schaefer, C.E., Lavorgna, G.M., Lippincott, D.R., Nguyen, D., Christie, E., Shea, S., O'Hare, S., Lemes, M.C., Higgins, C.P., Field, J., 2022. A field study to assess the role of air–water interfacial sorption on PFAS leaching in an AFFF source area. J. Contam. Hydrol. 248, 104001.
Schaefer, C.E., Lavorgna, G.M., Lippincott, D.R., Nguyen, D., Schaum, A., Higgins, C.P., Field, J., 2023. Leaching of perfluoroalkyl acids during unsaturated zone flushing at a field site impacted with aqueous film forming foam. Environ. Sci. Technol. 57 (5), 1940–1948.
Schaefer, C.E., Nguyen, D., Christie, E., Shea, S., Higgins, C.P., Field, J.A., 2021. Desorption of poly- and perfluoroalkyl substances from soil historically impacted with aqueous film-forming foam. J. Environ. Eng. 147 (2), 06020006.
Schaefer, C.E., Nguyen, D., Christie, E., Shea, S., Higgins, C.P., Field, J., 2022. Desorption isotherms for poly-and perfluoroalkyl substances in soil collected from an aqueous film-forming foam source area. J. Environ. Eng. 148 (1), 04021074.
Shea, S.M., Schaefer, C.E., Illangasekare, T., Higgins, C.P., 2025. Release of poly-and perfluoroalkyl substances from AFFF-impacted soils: Effects of water saturation in vadose zone soils. J. Contam. Hydrol. 104506.
Silva, J.A., Šimůnek, J., McCray, J.E., 2022. Comparison of methods to estimate air–water interfacial areas for evaluating PFAS transport in the vadose zone. J. Contam. Hydrol. 247, 103984.
Silva, J.A.K., Simunek, J., McCray, J.E., 2020. A modified HYDRUS model for simulating PFAS transport in the vadose zone. Water 12 (10), 2758.
Šimůnek, J., Šejna, M., Saito, H., Sakai, M., van Genuchten, M.T., 2013. The hydrus-1D software package for simulating the movement of water, heat, and multiple solutes in variably saturated media, version 4.17. Univ. Calif.- Riverside Res. Rep. 3, 1–342.
Smith, J., Brusseau, M.L., Guo, B., 2024. An integrated analytical modeling framework for determining site-specific soil screening levels for PFAS. Water Res. 252, 121236.
Stults, J.F., Choi, Y.J., Schaefer, C.E., Illangasekare, T.H., Higgins, C.P., 2022. Estimation of transport parameters of perfluoroalkyl acids (PFAAs) in unsaturated porous media: critical experimental and modeling improvements. Environ. Sci. Technol. 56 (12), 7963–7975.
Stults, J.F., Schaefer, C.E., Fang, Y., Devon, J., Nguyen, D., Real, I., Hao, S., Guelfo, J.L., 2024. Air-water interfacial collapse and rate-limited solid desorption control Perfluoroalkyl acid leaching from the vadose zone. J. Contam. Hydrol. 265, 104382.
USEPA, 1996. Soil screening guidance: User's guide. Office of Solid Waste and Emergency Response.
USEPA, 2024. Final PFAS National Primary Drinking Water Regulation. Technical Report, United States Environmental Protection Agency, URL: https://www.epa.gov/sdwa/and-polyfluoroalkyl-substances-pfas.
Vahedian, F., Silva, J.A., Šimůnek, J., McCray, J.E., 2024. Influence of kinetic air-water interfacial partitioning on unsaturated transport of PFAS in sandy soils. Sci. Total Environ. 957, 177420.
Wallis, I., Hutson, J., Davis, G., Kookana, R., Rayner, J., Prommer, H., 2022. Model-based identification of vadose zone controls on PFAS mobility under semi-arid climate conditions. Water Res. 225, 119096.
Weston Solutions, Inc., 2022. Addendum-3 facility-specific work plan/uniform federal policy - quality assurance project plan. Unpublished consulting report.
Zeng, J., Brusseau, M.L., Guo, B., 2021. Model validation and analyses of parameter sensitivity and uncertainty for modeling long-term retention and leaching of PFAS in the vadose zone. J. Hydrol. 127172.
Zeng, J., Guo, B., 2021. Multidimensional simulation of PFAS transport and leaching in the vadose zone: Impact of surfactant-induced flow and subsurface heterogeneities. Adv. Water Resour. 155, 104015.
Zeng, J., Guo, B., 2023. Reduced accessible air–water interfacial area accelerates PFAS leaching in heterogeneous vadose zones. Geophys. Res. Lett. 50 (8), e2022GL102655.
Zhang, Y., Schaap, M.G., 2017. Weighted recalibration of the Rosetta pedotransfer model with improved estimates of hydraulic parameter distributions and summary statistics (Rosetta3). J. Hydrol. 547, 39–53.